Study of the iron borides. IV. Relation of bonding to structure and magnetic behavior from photoemission experiments and *ab initio* calculations

David J. Joyner,* Oliver Johnson,* and David M. Hercules
Department of Chemistry, University of Pittsburgh, Pittsburgh, Pennsylvania 15260

David W. Bullett†
Cavendish Laboratory, University of Cambridge, Cambridge CB3 0HE, England

John H. Weaver
Synchroton Radiation Center, University of Wisconsin-Madison, Stoughton, Wisconsin 53589
(Received 23 December 1980)

Angle-integrated-photoelectron-spectroscopy measurements with synchrotron radiation ($15 \leq h\nu \leq 160$ eV) have been performed on the interstitial compounds Fe_2B (iron subboride) and FeB (iron monoboride). They show the iron states for FeB within ~4 eV of E_F and boron states at 6.6 eV (B 2*p*), 10.5 eV (B 2*sp* bonding), and 14.0 eV (B 2*s*). The boron states for Fe_2B are less intense, with B 2*s* nearer E_F, and with greater overlap of B 2*p*–Fe 3*d* states. When corrections are made for relaxation effects there is a good agreement between the experimental photoelectron-emission data, the boron states observed in soft-x-ray-emission boron-*K* measurements, and the Fe and B states from an *ab initio* calculation. Electronic-structure models are proposed for Fe_2B and FeB which differ from earlier charge-transfer models. These include a change in the Fe 3*d* configuration (and valence band), a provision for covalent bonding in the boron chain of FeB, greater Fe 3*d*–B 2*p* interaction in Fe_2B than in FeB, and a predominantly metallic binding in both borides. This model accounts for the metallic nature, the brittleness, the ferromagnetism, and the local moments of the iron borides, and also appears applicable to amorphous Fe-B compounds (metallic glasses).

I. INTRODUCTION

The iron borides, Fe_2B (iron subboride) and FeB (iron monoboride), belong to the important class of interstitial compounds formed by small metalloid atoms being placed in the interstices of the larger transition-metal crystal structure.[1-3] These interstitial boron atoms distort the iron crystal structure as shown in Figs. 1 and 2. Also, there are interesting changes in physical properties[3-5]: The iron borides are extremely hard and brittle although their melting points are close to that of iron, they are ferromagnetic with smaller local moments than for iron,[6] and they show the electrical conductivity and luster typical of metals. These are important materials for several reasons: Crystalline Fe_2B and FeB phases have been found in the surface of boride-doped steels, and they improve the wear and chemical resistance resulting from this treatment[7-9]; they are also of possible interest as heterogeneous catalysts.[10-12] In addition, the iron borides provide an insight into the commercially important amorphous iron-boron alloys (glasses).[13]

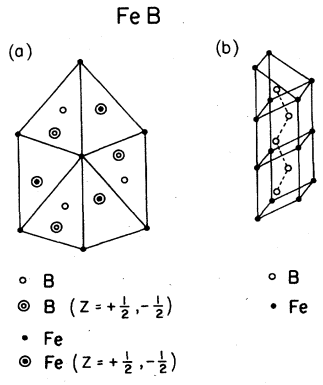

FIG. 1. Crystal structure of FeB: (a) Projection on (100) plane; (b) section perpendicular to (a), showing boron chains.

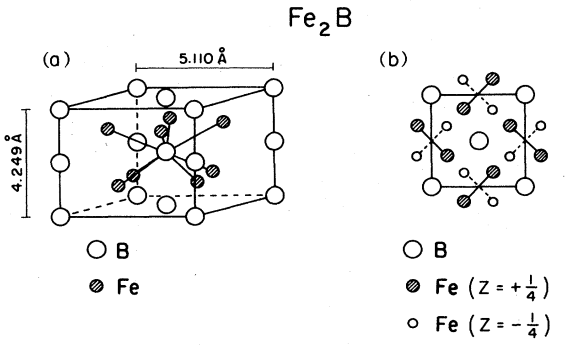

FIG. 2. Crystal structure of Fe_2B. Part (b) is a projection on a (110) plane illustrating the tetrahedral arrangement of Fe.

In the present paper the valence states of iron and boron are revealed by angle-integrated-photoelectron measurements using synchrotron radiation, by *ab initio* calculations, and by soft-x-ray-emission spectroscopy (SXS). By combining these data with our earlier measurements of core levels and x-ray-photoemission (XPS) valence bands[14,15] and studies of the iron boride's ferromagnetism,[16] we are able to give a description of their bonding and electronic structure. This scheme is different from models of earlier workers,[17-21] but is more accurate since by the use of spectroscopy and calculations, we are able to directly identify the Fe-derived and B-derived valence-band features. The work resolves much of the controversy surrounding the nature of bonding in these materials, a controversy resulting from a variety of studies over the years.[22,23] It explains many of the iron borides' physical properties including their magnetic behavior. In particular, it shows the inadequacy of simple models which require charge transfer from one component to the other.

II. EXPERIMENTAL

The Fe_2B and FeB samples used in this study were in the form of rectangular blocks $3\times3\times10$ mm^3, which were cut from high-purity ingots; preparation was described previously.[14] Preparation of the Fe_2B single crystals was previously described by Taga.[24]

The photoemission experiments were performed using synchrotron radiation from the 240-MeV electron storage ring Tantalus I at the University of Wisconsin, Madison. The samples were mounted in an ultrahigh-vacuum chamber equipped with a sample cleavage device, x-y-z-θ manipulator and double-pass CMA (used at a pass energy of 25 eV). The experimental configuration has been described previously.[25] The radiation was monochromatized by a "grasshopper" 2-m grazing-incidence monochromator and the experimental resolution, a combination of the monochromator output linewidth and the resolution of the analyzer, was as follows: 25–55 eV photon energy (0.4-eV resolution), 60 (0.48), 70 (0.66), 80 (0.86), 90 (1.1), 100 (1.3), 120 (1.9), 140 (2.6), and 160 (3.4). In the Fe_2B experiments using photon energies below 35 eV, a Seya-Namioka monochromator was used and resolutions of ~0.4–0.6 eV were obtained. In all the photoemission experiments the samples were cleaved at $\sim7\times10^{-11}$ Torr. Being very brittle, the FeB and Fe_2B samples were easily broken. The single crystals of Fe_2B did not cleave neatly, and irregular surfaces were obtained. A pressure burst to $\sim5\times10^{-10}$ Torr was observed during fracture, but the pressure fell immediately to the operating value, $\sim7\times10^{-11}$ Torr.

No specific surface analyses of the surfaces prepared *in situ* for photoemission were made, but it was previously shown[14] by XPS that the bulk crystals were free of contaminants,[26-29] and no chemisorption feature was observed. The soft-x-ray-emission data reported in this paper were obtained at the National Bureau of Standards, Washington, D. C., and a report of their measurement[30] is planned to appear elsewhere.

III. CALCULATIONAL DETAILS

The calculation of the electronic structure of these materials was based on an atomic-orbital method which has already established its validity in applications to a wide variety of transition-metal compounds, especially chalcogenides and metallic glasses. Details of the method can be found elsewhere.[31]

The basis in this case consisted of the $2s$ and $2p$ orbitals on boron sites and $4s$, $4p$, and $3d$ iron atomic states. The usual approximation to the exchange-correlation potential was adopted, depending on the local density of electron charge resulting from overlapping atomic charge densities in the crystal, with the proportionality constant α set to 0.7. The charge density in the solid was set up from neutral atoms, using an iron configuration $4s^{0.5}4p^{0.5}3d^{7.0}$ in order to start from a d-orbital atomic occupation roughly consistent with the resultant Fe configuration in the crystal. For the boron atoms the basis states and atomic potential were calculated for the ground-state s^2p^1 configuration. In fact, it emerged from the calculation that the occupied configuration of the boron atoms in FeB is much closer to s^1p^2, but the change does not modify the orbital self-energies or interatomic matrix elements sufficiently to alter significantly the resulting densities of states in these materials. The orbital self-energies are displayed in Table I. From the shifts relative to these isolated atom levels, the degree of bonding in the various regions of the projected densities of states can be assessed.

Only two-centered interactions were included in the calculation. These may be calculated by numerical integration for a small, discrete set of interatomic separations and then interpolated for

TABLE I. Valence-orbital energies for isolated atoms (eV).

	$Fe(s^{0.5}p^{0.5}d^{7.0})$	$B(s^2p^1)$	$B(s^1p^2)$
d	−5.7		
p	−3.2	−5.6	−5.7
s	−6.1	−10.9	−11.1

any intermediate distances which may arise in any complicated structure. Given these matrix elements it is simple (within the two-center approximation) to set up the secular equation in the Bloch basis appropriate to any given crystal structure and hence solve for the electron band structure $E_n(\vec{k})$. Because of the large unit-cell size of these materials, we plot in the figures below, not the dispersion of individual bands in $\vec{k}$ space but only the density of electron states as a function of energy. For the iron borides this involved diagonalizing fairly large matrices (e.g., 52×52 for FeB). Only a relatively small set of 24 regularly spaced $\vec{k}$ points in the Brillouin zone were sampled and the results were smoothed by a Gaussian function of half width 0.2 eV. Errors introduced by the small size of the sampling-point set are most severe at the highest binding energies in the valence band, where the density of states is very small, coming almost entirely from boron s states and only from $\vec{k}$ points near the center of the Brillouin zone. Thus, there is no doubt that with more complete sampling the s band below about -17 eV would tail off much more smoothly than in the figures below.

For FeB, components of the local densities of states projected on individual orbitals were calculated, in addition to the total density of states, in order to elucidate the contributions of the various atomic orbitals in different energy ranges. In this calculation, overlap charges were assigned equally between the respective orbitals as discussed elsewhere.[31] Summing over the occupied states it was found that the two atomic components were essentially neutral. The boron valence configuration was approximately $s^{0.9}p^{2.3}$, while the iron $3d$ occupation was very close to the $3d^7$ configuration assumed at the start. Thus, we would not expect corrections for self-consistency to be particularly significant. Boron densities of states were also calculated for a single boron chain taken from the FeB structure and for interacting boron chains. Each was calculated from sampling 512 regularly spaced $\vec{k}$ points in the Brillouin zone.

IV. RESULTS

A. Synchroton photoemission spectra of FeB and Fe_2B

The angle-integrated-photoemission valence-band spectra of FeB are shown in Figs. 3 and 4. Those of Fe_2B are shown in Fig. 5. The energy scales are referenced to the Fermi level and the emission intensities are plotted in arbitrary units. The relatively high secondary electron background reflects the irregular fractured surface of the samples.

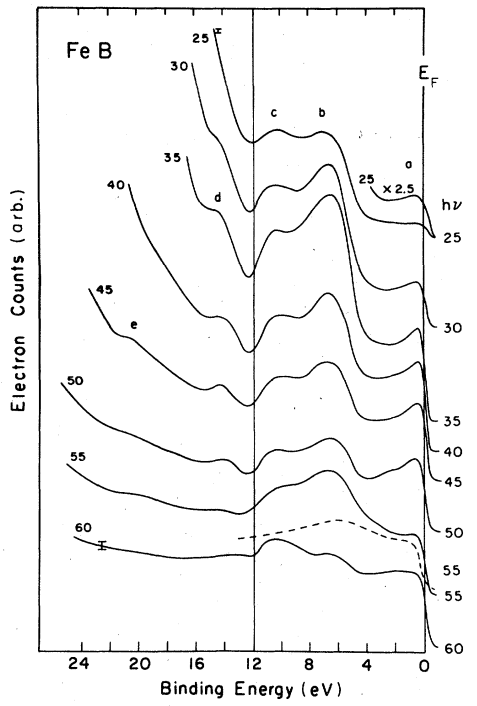

FIG. 3. Photoemission spectra of polycrystalline FeB for $25 \leq h\nu \leq 60$ eV. As discussed in the text the bands within 3 eV of E_F are Fe-$3d$ derived, peaks b and c are predominantly B $2p$, and peak d represents B $2s$. At 60 eV the Fe $M_{23}VV$ Auger peak coincides with peak c of FeB, thus causing an apparent reversal of intensities of peaks b and c. Dotted curve is for Fe_2B at $h\nu = 55$ eV.

1. FeB

The FeB photoemission spectra (Figs. 3 and 4) reveal a d-like band (peak a) at ~0.6 eV below E_F and a high density of states at E_f, consistent with the metallic properties of iron monoboride. However, at low photon energies ($h\nu < 50$ eV) the spectra are dominated at higher binding energies by the doublet $b+c$ at 6.6 and 10.5 eV. There is also a peak (d) at ~14 eV. As the photon energy is increased the intensity of the doublet falls smoothly with respect to the d band, and the relative intensities of peaks b and c of the doublet also change.

At a photon energy of 55 eV there is strong enhancement of peak b and at $h\nu = 60$ eV there is a reversal of the relative intensities of peaks b and c. At $h\nu = 53.4$ eV (the binding energy of the Fe $3p$ core level[14]), Auger emission overlaps the valence bands. The energy of an Auger electron transition XYZ is given by

$$E(XYZ) = E(X) - E(Y) - E(Z) - U_{\text{eff}}(YZ, S),$$

where $E(X)$, $E(Y)$, and $E(Z)$ are the one-electron

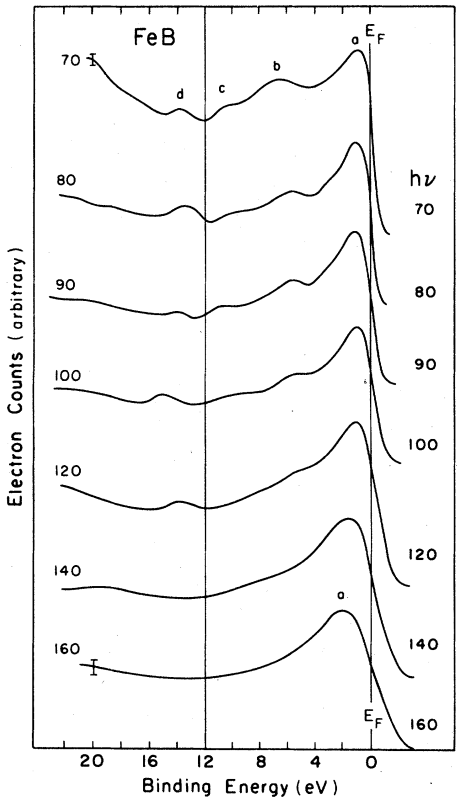

FIG. 4. Same as in Fig. 3 except values are now $70 \leq h\nu \leq 160$ eV.

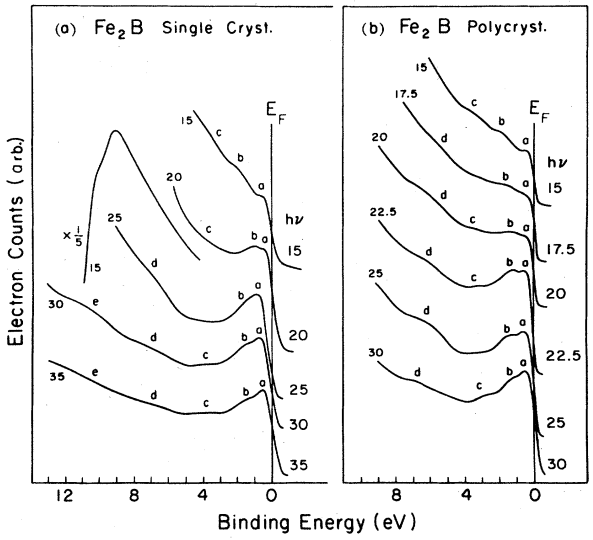

FIG. 5. Photoemission spectra of polycrystalline Fe_2B for $15 \leq h\nu \leq 30$ eV. Peaks a and b are Fe-3d derived and peaks c, d, and e are boron derived. In (a), the single-crystal samples did not cleave to produce a single face.

binding energies of the individual levels contributing to the transition, and U_{eff} represents the total additional energy required to create two holes in a final state, S, over that expected from the one-electron binding energies $E(Y)$ and $E(Z)$. The factor U_{eff} may thus be determined by comparison of Auger peak positions with those expected on the basis of single-electron transitions involving the appropriate valence densities. We have determined U_{eff} for the iron borides using the x-ray-excited Fe L_3VV transition, and have obtained a value of 1.6 eV for both borides.[32] Antonides and Sawatzky[33] and Yin *et al.*[34] obtained similar values of U_{eff} for iron. For the Fe $M_{23}VV$ emission, the kinetic energy will thus be $(53.4 - 1 - 1 - 1.6)$ eV $= 49.8$ eV, assuming that only the Fe 3d part of the valence band is probed due to the local nature of the Auger process. Note that the M_{23} levels (Fe $3p_{1/2,3/2}$) are seen as an unresolved doublet (spin-orbit splitting is 1.6 eV).[34(a)]

Thus, at 55-eV photon energy, the $M_{23}VV$ transition appears at ≃5-eV binding energy, exactly underneath peak b of the FeB valence density of states. At 60 eV the $M_{23}VV$ peak has moved by 5 eV to superimpose peak c of the FeB valence band (see Fig. 3), and contributes to the apparent reversal of relative intensities of b and c at this photon energy. This conclusion is corroborated by the appearance in the Fe_2B valence spectrum at 55-eV photon energy of an intense peak at the same position of peak b of the FeB spectrum (Fig. 3). No intense feature is seen in the Fe_2B spectra at this position for any other photon energy. At higher photon energies the $M_{23}VV$ transition moves to higher binding energies referenced to E_F, and is seen to be a single asymmetric peak of several electron volts at half width.

Apart from the above intensity changes there is little change with photon energy in the peak shape or position of FeB band a, the doublet $(b+c)$, or peak d. It will be shown below that peak a represents the Fe 3d local density of states while the others (b, c, and d) are various boron 2s2p densities.

2. Fe_2B

The Fe_2B spectra (Fig. 5) exhibit two peaks (labeled a and b) at ~0.8 and 1.4 eV below E_F, respectively. Fe_2B spectra also show small peaks labeled c, d, and e (at ~4, 6, and 10.5 eV, respectively), and there is little dependence of spectral features on photon energy.

The ultraviolet photoelectron spectra (UPS) of polycrystalline Fe_2B are nearly identical to those obtained from a single crystal; however, the latter did not cleave neatly and several crystal planes were exposed.

B. Band-structure calculations for FeB

The density of states of iron monoboride resulting from the *ab initio* band-structure calculation, including the total density of states and the projected Fe 3*d*, B 2*s*, and B 2*p* state densities, are shown[35] in Fig. 6. The valence band of FeB is dominated by Fe-3*d*-derived states within ~5 eV of E_F. The B-2*s*-derived bands dominate ~12 eV below E_F, and the B 2*p* states contribute strongly at ~4 and ~8 eV below E_F. The B 2*p* density is considerably greater than that of the B 2*s*. Both consist of essentially two bands, one being much larger than the other. The *l*-projected density of states were not determined for Fe_2B because of the large size of the unit cell.

The density of states determined for single boron chains in the FeB structure are remarkably featureless, but there is a very sharp low-energy edge of the *s* band at ~9 eV below E_F. The sharpness of the low-energy cutoff must reflect the weakness of the boron interchain interactions compared to the intrachain interactions, i.e., the quasi-one-dimensional aspect of the structure.

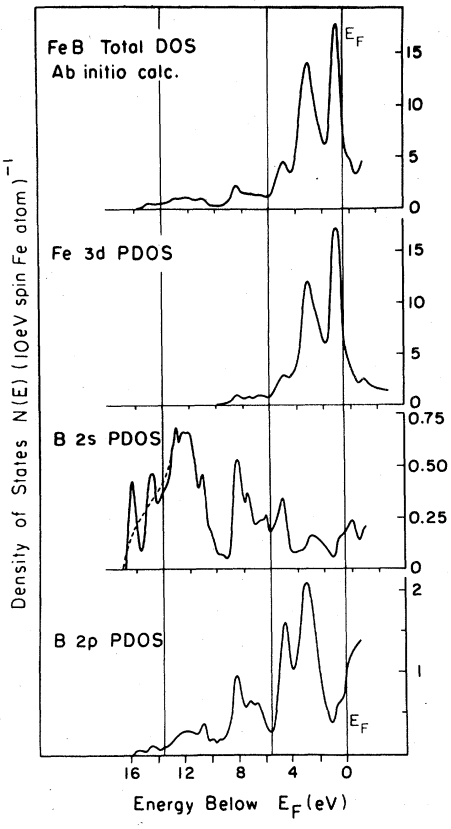

FIG. 6. *Ab initio* calculation for FeB with local density of states of iron and boron valence bands. The structure at high energies for the B 2*s* density of states is discussed in footnote (Ref. 35). (P)DOS represents (partial) density of states.

V. DISCUSSION

A. Iron borides Fe 3*d* valence bands

1. Fe 3d valence-band density of states

The valence bands of FeB and Fe_2B obtained by XPS (Ref. 14) are shown in Fig. 7(a). The valence bands of the two borides are compared with that of iron after background subtraction. It was previously noted[14] that these spectra do not show boron states due to the low photoionization cross sections of B 2*s* and B 2*p* at ESCA (electron spectroscopy for chemical analysis) energies. The Fe 4*s* conduction band is of low intensity and structureless.[36] As shown in Fig. 7(a) the valence bands of the iron borides have more structure and are wider than those of Fe.

In Fig. 7(b) we compare the present photoemission spectra for $h\nu \simeq 35$ eV to an analogous spec-

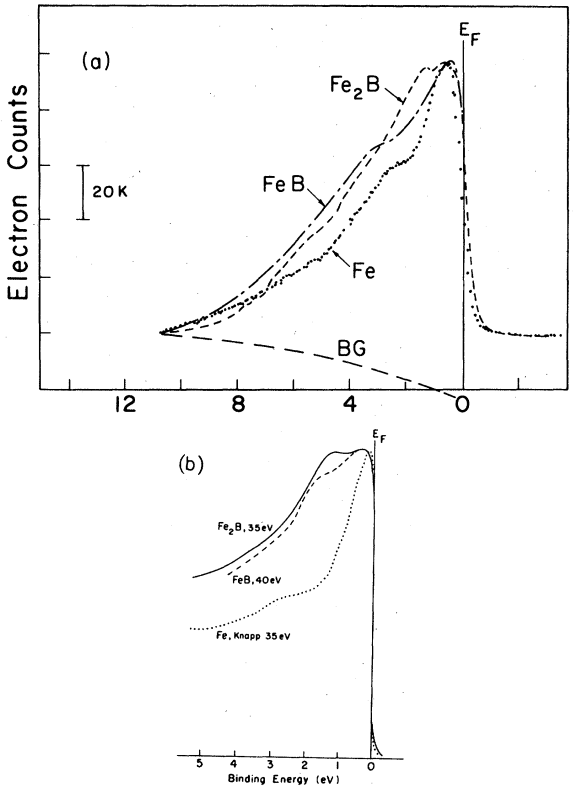

FIG. 7. (a) Comparison of XPS spectra of Fe, Fe_2B, and FeB. Fe 3*d* valence bands are from Ref. 13. (b) Comparison of photoemission spectra of Fe_2B and FeB with that for Fe (Ref. 34). Fe peak is shifted to align with peaks of Fe_2B and FeB. BG is the background. The synchrotron photon energies used in each case are marked.

trum for elemental Fe.[37] The same relative differences in the shapes of the 3*d* density of states of Fe, Fe_2B, and FeB are seen in these spectra as in the x-ray-excited valence bands [Fig. 7(a)]. Also, the photoemission spectra of Fig. 7(b) are typical of those for FeB and Fe_2B in the photon energy range 20–160 eV. From this, one may conclude (1) Final-state effects are unimportant in the angle-integrated-photoemission spectra of the iron borides, and (2) the boron 2*s*-2*p* contribution to the valence band within ~5 eV of E_F is overwhelmed by the Fe 3*d* bands.[38,39]

Figure 8 compares our valence-band spectra with Fe 3*d* local densities of states calculated by the *ab initio* method. The XPS valence bands in iron[14] are compared [Fig. 8(a)] with the calculation by Callaway and Wang[40] for ferromagnetic iron, which has been shown to reproduce the experimental curve well if various corrections are made to the density of states shown here.[41] Comparison of the present calculation for iron with that of Wang and Callaway, indicates that the present paramagnetic calculation for iron reasonably reproduces the observed spectrum although the splitting for the two major densities is too large [Fig. 8(b)]. This may be attributed to lack of consideration of magnetic exchange in the paramagnetic calculation of the *d* band, which produces separate spin-up and spin-down densities. An exchange energy in iron[42] of 1.5 eV would place a spin-down band in the region where the present calculation shows a minimum, and would thus give closer agreement with experiment.

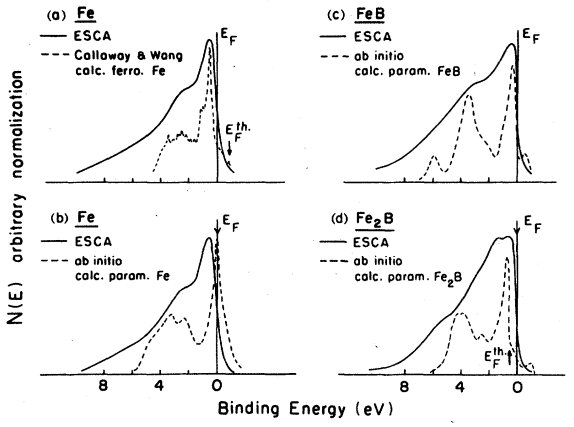

FIG. 8. Comparison of calculated Fe 3*d* densities of states with XPS Fe 3*d* spectra. (a) Iron—calculation by Callaway and Wang (Ref. 37). (b) Iron—present *ab initio* results. (c) and (d) FeB and Fe_2B—present *ab initio* results compared (for Fe_2B, the total density of states is presented). E_F is the calculated Fermi level; some of the calculated curves have been shifted as shown so that major features align with experimental spectra.

For FeB, comparison of the calculated paramagnetic band structure with the XPS valence band [Fig. 8(c)] shows reasonable agreement, the main peaks at ~1 and ~3.3 eV being reproduced despite the ferromagnetism of FeB. However, this is consistent with the much lower magnetic moment in FeB ($0.95\mu_B$ per iron[21]), which would give a smaller exchange energy in the *d* band than in iron, so that the majority and minority bands would be much closer together (i.e., near the paramagnetic case). For Fe_2B [Fig. 8(d)] the paramagnetic calculation shows the ~1-eV peak and reproduces most of the band shape except the peak at ~2.2 eV. This peak may be due to a magnetic feature arising because of the large local moment of $1.62\mu_B$ on iron in Fe_2B,[20] so that the majority and minority *d* bands are quite well separated, closer to the case of iron than FeB.

Comparison of photoemission data and band-structure calculations suggests that the main differences in 3*d*-valence-band densities of states in iron and the iron borides are due to differences in the ferromagnetic properties and structure-induced electronic changes in the materials. The same conclusion was reached in a previous consideration[15] of the detailed occupancy and degeneracy of the iron 3*d* orbitals based on charge- and spin-density data.

2. *Iron local valence orbital symmetry*

The photoionization-cross-section dependence of orbitals in a solid is known to be essentially the same as for the same orbitals in a free atom,[43,44] so it can be used as a fingerprint of orbital symmetry character.[45] This has been found for both core and valence orbitals; for example, the dependencies for 3*d* and 4*d* valence bands of certain metals agree well with atomic calculations for Kr 3*d* and Xe 4*d*.[43,46]

We have measured the peak areas of the assigned Fe 3*d* band features in the iron borides as a function of photon energy (from Figs. 3, 4, and 5). For Fe_2B, in which the boron states are apparently of very low intensity, the Fe 3*d* peaks were taken as the whole of the valence band (Fig. 5) after subtraction of a curved background due to secondary electrons. For FeB, however, the boron emission was large at low photon energies, and their low-binding-energy tail overlapped with the 3*d*-4*s* edge of the iron valence density. It was therefore necessary to attempt to resolve these features. This was done as shown in Fig. 9, where the spectra have first had a curved background subtracted. This analysis was performed by assuming (1) that the low-binding-energy edge of the boron states (in the region 4–6 eV) was Gaussian,

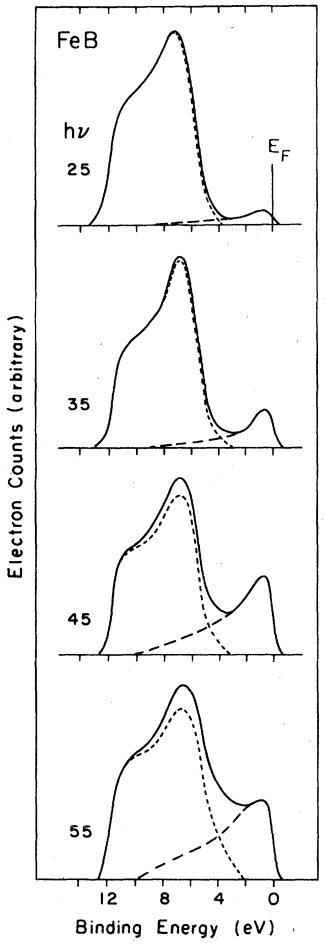

FIG. 9. Resolution of components of polycrystalline FeB UPS valence bands. Curved backgrounds fitted from Fig. 3 have been subtracted from the photoemission spectra. Short dashed line shows the boron states. Long dashed line shows the Fe 3*d* valence band whose shape is assumed constant with photon energy, by analogy with Fe_2B (Fig. 5) whose valence band is not complicated by boron states.

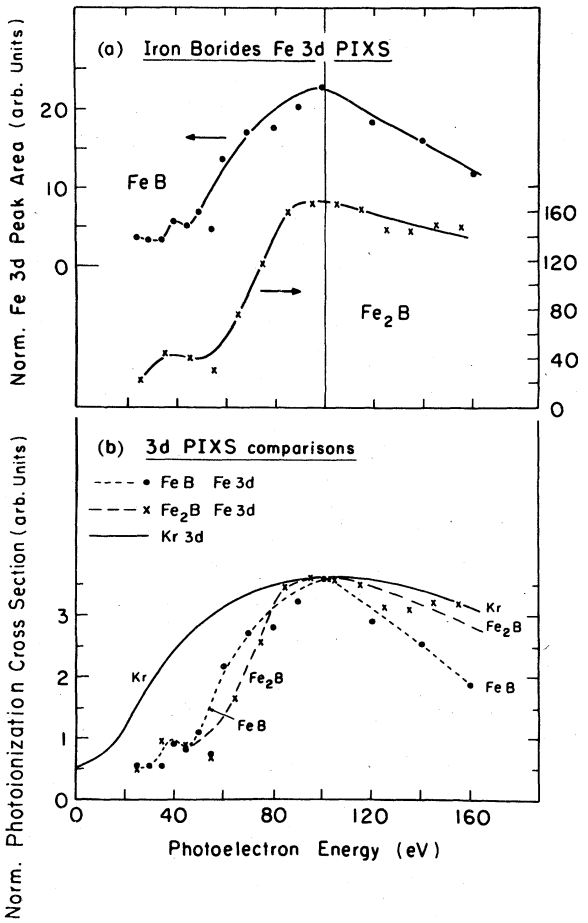

FIG. 10. Photon-energy dependences of FeB and Fe_2B Fe 3*d* cross sections. PIXS is the photoionization cross section. (a) Iron Borides Fe 3*d* PIXS. Note that although the intensity units are arbitrary, the cross-section dependences are scaled consistently with one another and with the boron state cross sections of Fig. 16. (b) Comparison of FeB and Fe_2B PIXS with Kr 3*d* PIXS (see text). All curves scaled to same intensity at 100-eV maximum.

as seen in Fig. 9 at 25-eV photon energy, where the boron states are pronounced, and (2) that the iron states (3*d* and 4*s*) extend to ~10 eV as shown by the XPS valence bands [Fig. 7(a)], and (3) that their shape does not change with photon energy.

The cross-section dependences are shown in Fig. 10. In part (a) the results for the two borides are shown on an intensity scale which is normalized to the photon flux (assumed proportional to the known electron current in the storage ring), the output of the monochromator (calibrated with a gold target), and the transmission of the CMA.[47] Thus, although the units are not absolute, the experimental cross sections reported here for the two boride Fe 3*d* bands and the boron valence bands (*vide infra*) are accurate with respect to one another. It is seen that the Fe 3*d* cross section at maximum is much higher in Fe_2B than FeB [Fig. 10(a)] in agreement with the higher iron stoichiometry of Fe_2B.[48]

In Fig. 10(b) the relative Fe 3*d* cross sections in the iron borides are compared with an atomic calculation for Kr 3*d*. All peaks have been normalized to have the same maximum intensity. The curves show essentially the same shape, and the obvious conclusion is that, to a first approximation, the Fe_2B and FeB cross sections show a dependence which is typical of 3*d* atomic orbitals, confirming the 3*d* nature of the iron-boride valence-band fea-

ture. This characteristic 3*d*-band cross-section behavior has also been seen in studies of Ga and As in GaAs.[48(a)]

B. Iron monoboride boron valence states

1. Resolution of B 2s2p valence states

In addition to the Fe 3*d* states considered above, the photoemission spectrum of FeB (Figs. 3 and 4) can provide considerable information about the boron valence states. As mentioned above, these states overlap the iron states and it is necessary to resolve them as shown in Fig. 9. The boron states were separated by subtracting the iron 3*d*-4*s* local density from the total spectrum and assuming that the remainder was due to boron. The peaks corresponding to peaks *b* and *c* of Figs. 3 and 4 are shown in Fig. 11(a) after this treatment. The spectra have been normalized to the same maximum as the 6.6-eV peak. They appear to contain two partially resolved Gaussian components (this is shown by the inset in which the low-binding-energy edge is compared with a Gaussian curve of the same width). The higher-binding-energy peak (*c*) increases in intensity compared with peak *b* as the photon energy is increased.

The boron peak (*d*) (Figs. 3 and 4), scaled to constant intensity, was compared for different photon energies. Because of its high-binding energy, it was only necessary to subtract a curved background to resolve this feature. Peak *d* is a single Gaussian peak at all photon energies, and it does not change shape or binding energy across the photon energy range, except for some broadening due to lower instrumental resolution at higher photon energies.

2. Analysis of boron valence states

In order to understand the boron valence states in FeB we compare [Fig. 11(b)] the photoemission peaks assigned as boron states (*b*, *c*, and *d* in Figs. 3 and 4) with the calculated 2*p* densities from the *ab initio* calculation described above. Also shown is the boron-*K* soft-x-ray-emission (SXS) spectrum of FeB. This should be compared directly with the B 2*p* local valence density of states since the dipole selection rule $\Delta l = \pm 1$ operating for SXS ensures that the process beginning with B 1*s* (i.e., *K*) emission probes only the B 2*p* part of the valence band.

The *ab initio* calculations give maxima in the partial densities of state (PDOS) at ~3.5 eV for B 2*p* and at ~12 eV for B 2*s*. These are to be compared with the photoemission peaks for boron states at 6.6, 10.4, and 14.0 eV. A shift of ~3 eV for the PDOS curves to higher energies would give

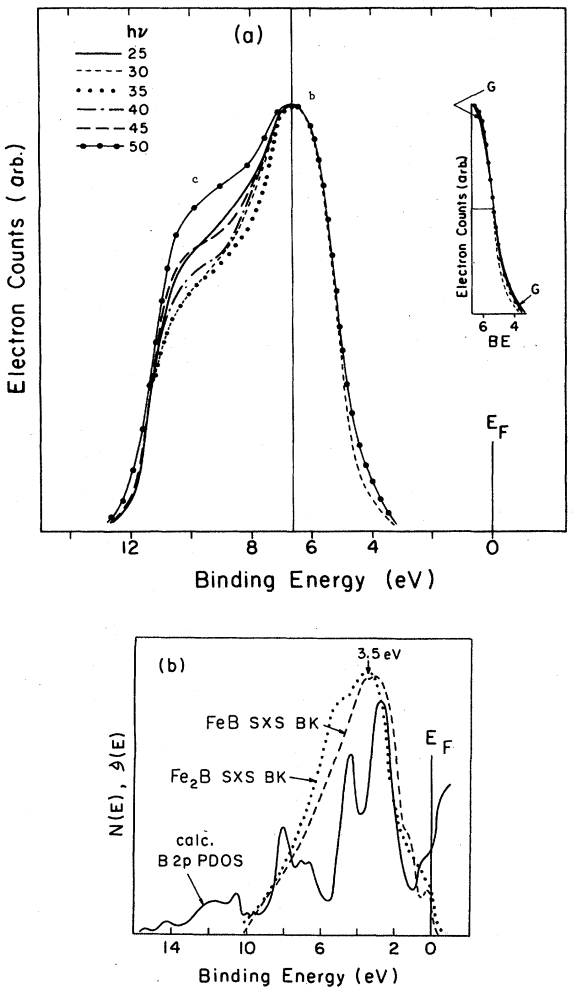

FIG. 11. (a) Boron states of polycrystalline FeB UPS valence bands. Boron components (peaks *b* and *c*) of the FeB valence bands (resolved in Fig. 9) are shown scaled to the same intensity at the 6.6-eV peak. Fe 3*d* density near the Fermi level is omitted from this figure. The inset shows an analysis of shape of low-binding-energy edge of boron states at photon energies of 30 and 50 eV. The spectral edges are shown to be close to Gaussian shape (the full line is the synthetic Gaussian of same half width). (b) Boron states of FeB(Fe_2B) from UPS, SXS, and *ab initio* calculation. Dashed curve: SXS B*K* emission (B 2*p*) of FeB; dotted curve: SXS B*K* emission of Fe_2B; full curve, *ab initio* calculation of FeB B 2*p* local density of states (Fig. 6). The calculated B 2*p* DOS and SXS boron-*K* spectrum come into agreement with the boron states determined in photoemission when the former are corrected for extra atomic relaxation.

a closer correspondence with the calculated peaks for 6.6 eV (peak *b*) and 14.0 eV (peak *d*).[49] Such a shift is reasonable in view of the difference between the calculated 2*p* energy at 5.6 eV for an isolated boron atom and the measured ionization po-

tential of 8.3 eV. Part of the difference is a relaxation energy—Koopmans' correction, but a strict Hartree-Fock calculation for the isolated atom does give a 2*p* energy level near the experimental ionization potential, so the 2.7-eV shift could be the error in the local ($\alpha = 0.7$) approximation to the exchange potential in the *ab initio* calculations.

In Fig. 12 the summed partial density of states for B 2*s* and B 2*p* is compared to the photoemission spectrum; for the summation the B 2*p* peak was aligned with peak *b* (shift of 3.0 eV) and the B 2*s* peak was shifted by the same amount. Figure 12 shows that there is agreement between the shapes of the calculated and experimental photoemission spectra. The differences in detailed shape are reasonable since the calculated curves do not include lifetime or instrumental broadening factors, matrix effects, or different photoionization cross sections for B 2*s* and B 2*p* orbitals.

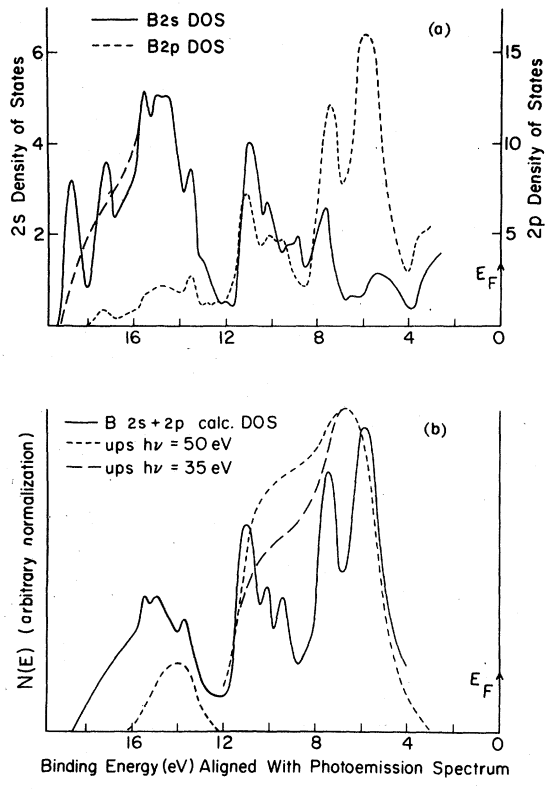

FIG. 12. Comparison of UPS FeB boron states with B 2*s* and B 2*p* calculated DOS. (a) *Ab initio* calculated B 2*s* and B 2*p* PDOS of FeB, with B 2*p* and B 2*s* shifted by 3 eV to align with photoemission peaks *b* and *d* (see Fig. 3). (b) Comparison of B 2*s* + B 2*p* summed DOS from a with boron photoemission states *b*, *c*, and *d*. The calculated band structure reproduces the experimental boron states quite well.

3. *Boron-valence-orbital symmetry*

Support for the assignment of peak *b* to B 2*p* and peak *d* to B 2*s* follows from a consideration of photoionization cross sections. These photoionization cross sections are shown for peaks *b* and *c* in Fig. 13, where they are compared with calculated cross sections for Ne 2*s* and 2*p* (Refs. 38 and 39), which are expected to show similar atomlike behavior to the boron 2*s*2*p* states (Sec. IV A 2). Boron intensities are assumed proportional to the photoionization cross sections and are normalized in the same way as the Fe 3*d* [see Fig. 10(a)].

The intensity of the boron states shows a monotonic decrease as the photon energy is increased. The points fall on a smooth curve except the point at 55-eV photon energy—this is because of the interference of an Auger peak, *vide supra*. This behavior is qualitatively similar to Ne 2*s* and Ne 2*p*,[38,39] although the calculation for these orbitals predicts a much smaller decrease across this photon energy range. The peaks assigned as boron states thus show a cross-section dependence consistent with *sp* symmetry; the cross section depends on the Fourier transform of atomic orbitals and the Fourier transform falls off much more rapidly for the large B than the small Ne. The different shape of the wave function is the probable source of the quantitative difference between boron data and the calculated data for neon.

The above assignment for peaks *b* and *d* is also consistent with the observed photoemission intensities. The relative proportions of 2*s* and 2*p* for the peaks *b*, *c*, and *d* are given in Table II. Since with increasing photon energy the cross section of 2*s* orbitals increases compared to 2*p* (because 2*s*

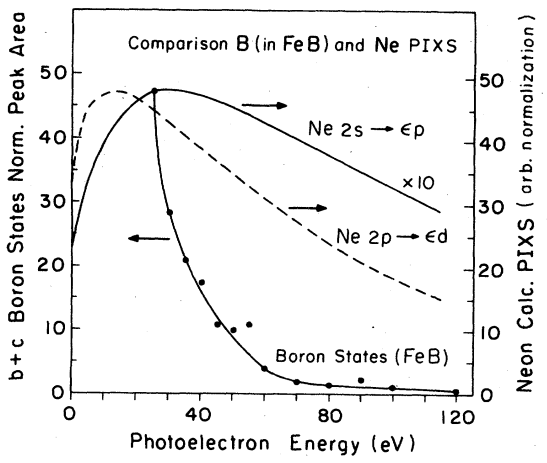

FIG. 13. FeB UPS PIXS of boron states. Boron states of FeB (peaks *b* and *c* of Figs. 3 and 4). PIXS compared with Ne 2*s* → ϵp and 2*p* → ϵd calculated PIXS (see text), ϵ representing the final-state channel.

TABLE II. Proportions of boron 2*s* and 2*p* orbitals in FeB valence bands; *ab initio* results.

Peak of UPS spectra[a]	Orbital content[b] %*s*	%*p*
b	14	86
c	28	72
d	67	33

[a] See Figs. 3 and 4; $b = 6.6$ eV binding energy, $c = 10.5$ eV, $d = 14.0$ eV.

[b] See Fig. 12. Peak *d* is assigned as essentially B 2*s*, and peak *b* as B 2*p*.

has a sharp oscillation arising from orthogonality to the core state), the relative intensities with photon energy should reflect the relative 2*s* to 2*p* composition. The intensity ratios *c* to *b* and *d* to *b* are shown in Fig. 14 and clearly increase in qualitative agreement with the *s* to *p* intensity ratio for Ne. A similar *s* to *p* cross-section increase across this energy range has been seen for C 2*s* to 2*p* of graphite[50] as shown also in Fig. 14. The higher value of the intensity *c* to *b* compared to *d* to *b* reflects the greater 2*p* content for peak *c*, and the greater slope for *c* to *b* results from the lower 2*s* content of peak *c* compared to peak *d*.

It is seen in Fig. 11(b) that there is close agreement between the SXS 2*p* density of states and the calculated 2*p* local density of states. Correction for the change of resolution with energy was not made, so intensity appears to fall off above 10 eV in the SXS data of Fig. 11(b). Thus, the B 2*p* energy from SXS data is 3.5 eV below E_F in agreement with the *ab initio* calculated value. A direct comparison to the photoemission data should not be made since a relaxation energy is involved in the SXS process which is not present in photoemission. This will be treated in detail in Sec. V D.

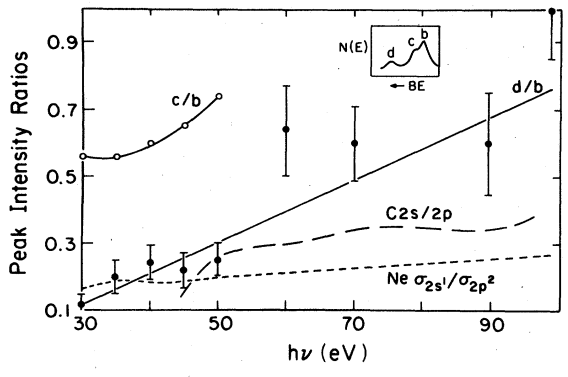

FIG. 14. Ratio of various photoionization cross sections for FeB. Ratios are based on intensities from Figs. 3, 4, and 11(a) of the boron states *b*, *c*, and *d*. Intensities are used instead of areas since peaks *b* and *c* are not deconvoluted, and there is no noticeable change in peak shape with photon energy. ○ is the *d* to *b* ratio, 0 is the *c* to *b* ratio, and *short dashed* line shows Ne 2*s* to 2*p* calculated for a $2s^1p^2$ population, adapted from Kennedy and Manson. (Ref. 39). *Long dashed* line is the ratio of experimental C 2*s* to C 2*p* cross sections in graphite (Ref. 50). The data confirm that peak *d* is essentially B 2*s* density and peak *b* essentially B 2*p* density.

C. Iron subboride boron valence states

The boron valence states of Fe_2B are of much lower intensity than expected from the differences in stoichiometric boron content between Fe_2B and FeB. This may be due to a different kind of bonding in Fe_2B which causes the boron states to be less distinct. Peaks *c*, *d*, and *e* of Fe_2B are the boron states by analogy with FeB (Figs. 3 and 4). Peak *c* would be largely B 2*p*, like the highest peak in FeB; peaks *d* and *e* would contain B 2*s* and B 2*p*, peak *e* probably being largely B 2*s*. The photoionization-cross-section behavior of the peaks in the photoemission spectra (Fig. 5) gives support for this assignment. Peaks *d* and *e* increase with respect to *c* at higher photon energies as expected by comparison with FeB (above). The soft-x-ray-emission B *K* spectrum of Fe_2B [Fig. 5(b)] is quite similar to that of Fe_2B [Fig. 11(b)], but with the maximum moved from 3.5 to 4 eV below the Fermi level, and with a shoulder at 5 eV. This is close to peak *c* of the UPS spectrum and suggests that this peak is essentially B 2*p* as was determined similarly for the highest-energy boron state of FeB.

The main difference between the boron states of Fe_2B and FeB would thus appear to be the shift upwards in energy of the Fe_2B peaks. The binding energies of these states will be discussed in Sec. V D and the significance of the results for the electronic structure of the iron borides in Sec. V E. However, these assignments for Fe_2B remain tentative since, because of the low intensities of the peaks, analysis of their orbital symmetries could not be made as for FeB; also, band-structure calculations to predict the boron density of states have not been performed.

D. Binding-energy shifts of iron borides valence states

Since the SXS emission for B 2*p* involves the B 1*s* core hole and photoemission of B 2*p* does not, there is an additional relaxation which must be taken into account in comparison of the two. Relaxation[51,52] due to boron valence electrons is estimated to be 2–3 eV, and correction for this would mean an increase in the B 2*p* energy. This is equivalent to the correction applied to the *ab initio* B 2*p*

calculations, where it was also considered that relaxation was involved. Thus, we propose that the FeB photoemission peaks show initial-state values, where the SXS and *ab initio* peaks are lowered by relaxation effects. There is good agreement of all the data when reasonable corrections are applied to the SXS data and the *ab initio* calculations.

As seen in Table III the positions of the boron valence states of Fe_2B and FeB as assigned here are in the same energy region as those states of other borides (ZrB_2 and LaB_6),[53,54] with B 2*p* at ~6 eV and B 2*s* at ~12 eV below E_F; also, the energy differences between B 2*s* and B 2*p* are similar at ~6 eV. Furthermore, the SXS results for ZrB_2 (Refs. 55 and 56) show the B 2*p* density at 3.5 eV exactly the same as in FeB, whereas the photoemission data showed the ZrB_2 B 2*p* peak to be at 6 eV.[53] The same discrepancy between SXS and photoemission energies is thus observed for ZrB_2 and FeB. On the other hand, as for Fe_2B the SXS and photoemission data agree for LaB_6.[54,57] There is also agreement between SXS and photoemission for the partly ionic compounds B_2O_3 and BN.[55,58-60]

A qualitative estimate of the gradation in B 1*s* relaxation effects can be made to clarify these observations. In B_2O_3 and BN there is electron transfer from boron to the anion, and the lower electron density around B leads to a small relaxation effect. The B_6 anion in LaB_6, although negatively charged, has electron deficient B–B bonds, and low relaxation is also expected. The boron layer structure in ZrB_2 leads to metallic properties and a high relaxation effect as in FeB is expected. Thus, relaxation effects are expected to have the gradation FeB, $ZrB_2 > Fe_2B > LaB_6$, B_2O_3, BN, and account for the observed B 2*p* energies.

E. Bonding and electronic structure of the iron borides: Relation to crystal structure, magnetism, and physical properties

The valence bands of the iron borides are shown schematically in Figs. 15(a) and 15(b) as based on our experimental results. Comparison to the model discussed by Perkins and Brown,[21] attributed originally to Lundquist,[17] shows that the latter is unable to describe the experimental observations. In particular, this model, shown in Figs. 15(c) and 15(d), predicts that the occupied states of FeB are almost entirely Fe 4*s*-3*d* derived with B 2*sp*-binding character within 2 eV of E_F. For Fe_2B they

TABLE III. Positions of boron valence bands of several boron compounds as revealed by photoemission, SXS, and calculation. APW stands for augmented plane-wave approximation and BE for the binding energy.

Compound		Boron valence states BE (eV) B 2*s*	B 2*p*	Δs-p	SXS B K energy (B 2*p*) (eV)	XPS B 1*s* BE (eV)
B atomic[a]		12.5	7.9	4.6		200.8
B_2O_3	XPS[b]	14.4	11.2	3.2	11[c]	191.3
BN	XPS[d]	11.4	8.3	3.1	9[c]	190.6
FeB	UPS[e]	14.0	6.6	7.4	3.5[f]	188
	ab initio calc.[e]	12.0	3.5	8.5		
Fe_2B	UPS[g]	10.5	4.0	6.5	4.0[h]	188
ZrB_2	XPS[i]	12.0	6.0	6.0	3.5[c]	188
	APW calc.	12.0	6.0	6.0		
LaB_6	UPS[j]	10.0	5.0	5.0	5.0[k]	188
	APW calc.[l]	10.0	5.0	5.0		

[a] At. Data 18, 243 (1976).
[b] Reference 58.
[c] Reference 55.
[d] References 58 and 59.
[e] Present work, see Figs. 3 and 4.
[f] Present work (McAlister *et al.*), see Fig. 11(b).
[g] Present work, see Fig. 5.
[h] Present work (McAlister *et al.*), see Fig. 5.
[i] Reference 53.
[j] Reference 54.
[k] Reference 57.
[l] Reference 60.

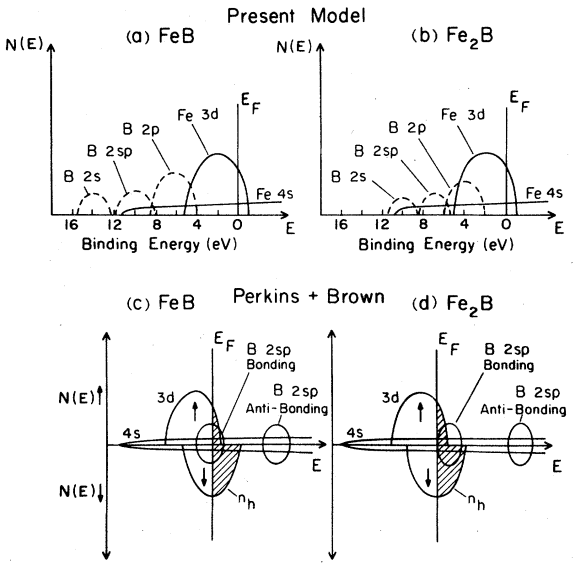

FIG. 15. Models for the valence-band structure of the iron borides (see text and Ref. 76). (a) and (b): Present model; (c) and (d): Perkins and Brown, Ref. 21. The band shapes are drawn schematically. In (c) and (d) n_h refers to the number of holes in the valence bands, indicated by cross hatching. The majority and minority bands are indicated by up and down arrows on the Perkins and Brown model but have been omitted from the diagram of our model for simplicity.

predict that the boron states are completely unoccupied. On the contrary, for FeB we find the B 2*s* band at ~14 eV, a hybridized B 2*sp* band at ~10 eV, B 2*p* structure at ~6 eV and the states within ~4 eV of E_F to be largely Fe 3*d* derived. For Fe_2B the B 2*p* and B 2*s* states are closer to E_F, and there is greater B 2*p*-Fe 3*d* overlap.

The boron valence orbitals in FeB appear to have hybridized to an sp^2 configuration. In the crystal structure of FeB, which has boron atoms winding in zigzag chains through the interstitial holes and a boron coordination number within the chain of two, these zigzag chains can be explained by the trigonal nature of sp^2 orbitals involving covalent boron-boron bonds. Each boron contributes two sp^2 electrons to its two boron neighbors, with the other sp^2 orbital not bonded to boron atoms. Several aspects of the FeB crystal structure support this view: (1) Strong boron-boron bonding within the chain is consistent with the short boron-boron distance of 1.78 Å which is within the range normally found for covalent B–B bonds; (2) the Fe–Fe distances are shorter in the axial direction in order to provide for 1.78-Å B–B distance; (3) the boron atoms are not located at the centers of the octahedra as in the case of interstitial anions, but are virtually in the plane of the irons, suggesting a stronger bonding between a boron and the neighboring boron atoms than between the boron atoms and the neighboring irons. Finally, our conclusions of covalent bonding within the boron chain of FeB are strongly supported by the neutron diffraction measurements of Perkins and Brown, whose difference (spin-) density maps taken within the plane of the boron chain showed a band of negative density passing along the chain.

In Fe_2B the boron states are less bonding than those of FeB, suggesting that the strong interaction between the boron atoms is not upheld when the boron concentration is lowered. This is consistent with the large B–B distance of 2.13 Å in Fe_2B. Also, the boron states of Fe_2B are nearer in energy to the iron 3*d* valence states so that iron-boron interaction would be expected to correspondingly increase in Fe_2B.

Since in FeB two of the three boron electrons per atom are used for bonding with other borons, at most one other electron is available for iron-boron bonding, suggesting that the latter interaction is much weaker than the in-chain interaction. In fact, we suggested previously[14] that 0.2 electron per boron is donated to the conduction band so only 0.8 electron per boron is left.

In view of these differences in the boron-valence-band structure of the two compounds it is of interest to consider the nature of boron-iron and iron-iron interaction in FeB and Fe_2B. This can be largely answered by considering the Fe 3*d* local valence states, the core-level photoemission data, and crystal structures. Boron-iron distances are in the same range in both compounds, suggesting a similar interaction between the elements. The iron-iron distances are also similar but with a variety of neighbor distances. The iron sublattice is not unlike elemental iron but is successively distorted from cubic structure by the addition of boron; in the case of Fe_2B one unit-cell dimension is elongated to give a tetragonal structure, and in FeB further distortion results in one of the primary angles being greater than 90° (orthorhombic structure). X-ray and neutron scattering measurements[20,21] indeed indicate that the type of iron–iron bonding in the iron borides is similar to that in the element, being composed of diffuse electron densities centered off lines joining the atomic centers. Since this is typical of bonding densities in many elemental metals we shall call it "metallic."[15] It seems that the interaction between iron and boron is also essentially metallic.

The core-level photoemission results presented in Paper I of this series[14] strongly support this picture. First, the unchanged iron- and boron-core-level binding energies in the two iron borides

compared with the elements show that the compounds do not have ionic character, but that the electron densities around iron in the iron borides are similar to those in iron itself. A similar electron density is supported by core-level energy-loss (plasmon) spectra.[14]

The core-level-binding-energy data and the present valence-band data also disprove the earlier rigid-band model for the valence electronic structure in which an increasing number of electrons was assumed transferred to iron from boron as the boron content increased. This would cause different core-level binding energies in the compounds, which was not observed in our study. The iron $3d$ valence bands of the compounds are similar, overlapping the Fermi level, showing a sharp Fermi edge and typical $3d$-band shape similar to iron. This indicates the metallic nature of iron is retained in the iron borides as suggested above. However, there are important changes in the iron $3d$ valence bands which we analyzed in detail in Sec. IV A. Both of the iron-boride $3d$ valence bands are wider than that of iron, and new features are seen in both compounds, namely, a shoulder at 3.3 eV in FeB and a peak at 1.4 eV in Fe_2B. It was shown above that these represent significant differences in the d-band density of states, related to crystal structure as well as to ferromagnetism.

Comparing Fe and the iron borides, increased distortion of the cubic iron lattice modifies the symmetry of the iron-atom nearest neighbors. This symmetry change alters the valence-band shapes, as observed in the photoemission spectra, and the apparent increase in bandwidth on going from Fe to Fe_2B to FeB is consistent with this progressive symmetry distortion. In fact, using such symmetry arguments and comparing with the spatial information in the d-electron distribution (from charge- and spin-density maps), we were able to determine[15] the energy ordering and occupancy of the various d orbitals.

The ferromagnetism of the iron borides is also reflected in the photoemission valence bands since the ferromagnetic coupling is associated with an exchange energy which energy splits the majority (spin-up) and minority (spin-down) bands. These bands are seen separately in photoemission with an energy separation related to the size of the local magnetic moments.[42,61] A new peak was observed in Fe_2B (at 1.4 eV) close to the Fermi level, probably due to exchange splitting, but no new features in FeB (which has a smaller exchange energy and different d-orbital occupancy). This ferromagnetic character is one of the most interesting properties of the iron borides. It is related to the size of the local magnetic moment—the number of unpaired electrons—on the iron atoms, so understanding of their magnetism requires a knowledge of the iron d-electron population.

The early rigid-band model suggested the following explanation for the iron-boride magnetic moments: Electrons are increasingly donated from boron sp to iron $3d$ bands as the boron content increases, and the magnetic moment is successively reduced as the minority band of Fe is filled. We have shown above that this model is incorrect and we seek an alternative explanation for the differences of magnetic properties.

The magnetic nature of the iron borides has been studied in detail by Perkins and Brown[21] using polarized neutron scattering to determine the magnetism and spatial variation of the iron $3d$ electrons as well as the conduction electrons. They deduced $3d$ local moments (μ_B) of 1.62 for Fe_2B and 0.95 for FeB. In both compounds the conduction electrons were found to contribute to the magnetization, being positively polarized with 0.28 μ_B per iron atom in Fe_2B and only 0.08μ_B per iron atom in FeB. In the electron density maps of Perkins and Brown[21] reversal of polarization on an iron atom occurs at distances greater than 1.3 Å from its center.

The problem of defining the local moment in Fe is exemplified in our recent measurement of the multiplet splitting of these compounds.[16] The Fe $3s$ splitting seen in XPS is related to the local magnetic moment through the exchange interaction between the core and unpaired valence electrons. We obtained moments of 2.3μ_B (Fe), 2.55μ_B (Fe_2B), and 2.05μ_B (FeB) which in the case of the borides are higher than those from neutron scattering (Fe_2B 1.62μ_B, FeB 0.95μ_B). Although it was concluded that these differences were due to electron correlation effects there still remains the problem of what part of the polarized electron density the technique is probing. Clearly, different techniques may give information about different parts of the magnetic electronic structure.

A more general problem closely related to this is whether the Fe $3d$ electrons can be described as localized or whether, as is widely accepted for iron metal, they are delocalized or itinerant.[62,63] This is a difficult and controversial point[64] but several papers supporting a view of metallic valence densities comprising *both* localized and itinerant d electrons have appeared in recent years.[65-69] Using such a model for the iron borides based on charge- and spin-density maps, we have determined[15] the following electron partitions for iron and the borides:

Fe: $|Fe^{8+}(d^6)_I(d^{0.5})_i,\ 1.5e_{tet}|_{bcc}$,

Fe_2B: $|Fe^{8+}(d^6)_I(d^{0.5})_i,\ 1.6e,\ \frac{1}{2}[(2p_z)^{0.8}B^{3+}(2s^2)]|_{C16}$,

FeB: $|Fe^{8+}(d^7)_I(d^{0.35})_i,\ 0.85e,\ (2p)^{0.8}B^{3+}(2s2p)|_{B27}$.

Here, the outer brackets indicate the repeating unit in the structure noted on the right of the bracket. The positive iron core (Fe^{8+}) is the argon shell in this case; subscripts l and i indicate d electrons localized around the iron core and itinerant d electrons, respectively. Beyond the first comma is the number of conduction electrons, and beyond the second comma (in the borides) is the valence electron configuration of boron. In this formalism, we propose that the magnetism of these materials is explained by their different d-orbital occupancies. These, likewise, are determined by the different partitioning of d electrons between localized electrons, more diffuse itinerant ones, and those donated to the conduction band. Thus, rather than boron donating electrons to the iron valence density, as in the rigid-band model, it donates charge to the conduction band (we determined 0.2 electron per boron) to give the observed conduction-band polarization.

In summary, the iron borides are understood by a metallic model in which the essentially diffuse metallic bonding between the iron atoms of elemental iron is retained in the borides. The effect of addition of boron is to distort the iron lattice, the distortion being greater the more boron that is added. Also, as the boron content is increased between Fe_2B and FeB the boron-boron interaction becomes considerably greater and causes covalent B–B bonding resulting in a two-dimensional boron chain winding through the interstitial holes. The interaction between iron and boron is correspondingly greater in Fe_2B than in FeB since in the latter the boron electrons are strongly bound to other borons. In Fe_2B then, the Fe-Fe and Fe-B interactions predominate, whereas in FeB it is the Fe-Fe and B-B interactions.

This picture suggests that the iron borides are "good" interstitial compounds and the covalent interaction between the boron atoms at higher concentration fits into the pattern observed for other borides: The fact that as boron concentration is increased, covalent B-B interactions become more and more predominant, is reflected in formation of chains (as in FeB), then nets, and finally three-dimensional structures similar to elemental boron.[22,23]

It is interesting to relate these crystalline iron borides to the iron-boron metallic glasses because of the importance of understanding the glasses' bonding nature. Most models of the structure of these materials assume that the local atomic bonding remains the same as in the crystalline material[70–72] while the long-range ordering is different. The highest concentration of boron which can be used to make an Fe-B glass is 25% (i.e., Fe_3B), so it is appropriate to compare these materials with our Fe_2B study. Since we determined that there was little B-B interaction in Fe_2B, the bonding of Fe_2B and these dilute glasses was likely to be similar.

Several recent reports have appeared on photoemission from iron-boron binary and ternary glasses and related cobalt glasses.[73–75] These compounds show similar trends in their electronic structures to the crystalline iron borides. For example, iron-boron glasses of different compositions[72] revealed Fe $3d$ bands different from iron metal, and there was no indication of charge transfer between iron and boron. The rigid-band model obviously does not apply to glasses. Also, a peak at 10-eV binding energy in XPS was attributed to boron. By comparison with our data for Fe_2B this is at the same energy as the B $2s$ peak of Fe_2B (the B $2p$ peak not being seen in XPS because of the low cross section). These results indicate essentially identical bonding structures in the iron-boron glasses and Fe_2B, i.e., "metallic" Fe–Fe and Fe–B bonding with no appreciable interaction between the borons. As in Fe_2B, the proximity in energy of the Fe $3d$ and B $2sp$ valence bands makes possible strong bonding interaction between the elements.

In an XPS study of amorphous $Fe_{80}B_{20}$ performed at much higher resolution[73] the glass Fe $3d$ valence band is similar to that of Fe_2B, being broader than elemental iron and showing similar evidence of two peaks near the Fermi level. As in Fe_2B, part of the valence-band structure is probably related to the ferromagnetism of $Fe_{80}B_{20}$. This is further evidence that the bonding and close-range atomic order in the iron-boron glass is similar to crystalline Fe_2B and that the d states are modified by the presence of boron.

The above description for the iron borides explains many of their properties which we have discussed previously.[14] One of the interesting properties is their great hardness and brittleness. The microhardness (kg/mm^2) of Fe_2B is 1340 and that of FeB 1650 (compare with iron, 70).[14] This may be related to the inhomogeneity of the electronic distribution. FeB is very inhomogeneous due to strong bonding in the boron chain which is along the c axis. The lack of B–B bonding in Fe_2B suggests a more homogeneous structure reflected in considerably lower microhardness and brittleness.

VI. CONCLUSIONS

Valence-band-photoemission results for Fe_2B and FeB are complementary to our earlier XPS measurements of the core levels and valence bands since in the latter the boron states were not

seen due to low cross sections at XPS energies. Combining these data with *ab initio* calculations and soft-x-ray-emission data, a detailed picture of the bonding and electronic structure in the iron borides has been formulated.[76] The use of synchrotron radiation with its continuously tunable photon energy allowed clear distinction between the iron and boron valence states. Monitoring their photoionization cross sections as the photon energy was changed, provided a check of their orbital symmetry.

The iron borides have been shown to be "typical" interstitial compounds, with boron occupying interstitial positions in a distorted iron lattice. The distortion is greater the higher the boron content; thus, iron has a cubic structure, Fe_2B is tetragonal, and FeB orthorhombic. The metallic iron-iron bonding found in iron, involving diffuse electron densities off lines joining the atomic centers, is retained in the iron borides. The bonding between iron and boron is also metallic but is stronger in Fe_2B than in FeB. The essential difference between the two compounds is that there is no boron-boron interaction in Fe_2B, but significant boron-boron interaction occurs for FeB, producing linear zigzag boron chains winding through the crystal with covalent trigonal sp^2 B–B bonds.

The valence-band structure of FeB and Fe_2B deduced from this work is different from the early rigid-band model or that based on neutron diffraction. We find that the iron 3*d* bands occur within 4 eV of the Fermi level while the boron bonding states occur at 6.6, 10.5, and 14.0 eV in FeB, and 4.0, 6.5, and 10.5 eV in Fe_2B. Our model explains many iron-boride physical properties, and their various *d*-electron distributions explain their ferromagnetism and local magnetic moments. Finally, the iron borides provide a fascinating example of the modifications of physical properties and electronic structure of a metal by interstitial addition of small metalloid atoms, a phenomenon of enormous importance in metallurgy and heterogeneous catalysis.

ACKNOWLEDGMENTS

Acknowledgment is made by D.J.J., O.J., and D.M.H. to the donors of the Petroleum Research Fund, administered by the American Chemical Society, for support of this research. The work of J.H.W. at the University of Wisconsin was supported by NSF Grant No. DMR 78 21080. We are grateful to the staff of the University of Wisconsin Synchrotron Radiation Center for excellent support. We are indebted to H. Taga of the National Research Institute for Metals, Tokyo, for providing the Fe_2B single crystals. Thanks are also due to A. J. McAlister and J. Cuthill of the National Bureau of Standards for generously performing the SXS experiments.

[1]B. Aronnson, T. Lundström, and S. Rundquist, *Borides, Silicides and Phosphides* (Wiley, New York, 1965).
[2]L. H. Bennett, A. J. McAlister, and R. E. Watson, Phys. Today 30, (9), 34 (1977).
[3]*Boron and Refractory Borides*, edited by V. L. Matkovich, (Springer, Berlin, 1977).
[4]I. I. Kostetskii, S. N. L'vov, and Yu. A. Kunitskii, Izv. Akad. Nauk SSSR, Neorg. Mater. 7, 951 (1971).
[5]Yu. A. Kunitskii and E. V. Marek, Poroshk. Metall. 11, 56 (1971).
[6]M.—C. Cadeville and E. Daniel, J. Phys. (Paris) 27, 449 (1966).
[7]N. I. Timofeeva, M. Ku. Levinskaya, and Z. I. Krainova, Izv. Akad. Nauk SSSR, Neorg. Mater. 6, 164 (1970).
[8]H. J. Goldschmidt, *Interstitial Alloys* (Plenum, New York, 1967).
[9]H. C. Child, *Surface Hardening of Steel, Engineering Design Guides*, No. 37 (Oxford University Press, London, 1980).
[10]J. F. Taylor and J. K. A. Clarke, Z. Phys. Chem. N. F. 103, 216 (1976).
[11]R. J. Madix, J. Vac. Sci. Technol. 13, 253 (1976).
[12]G. Wedler and D. Borgmann, J. Catal. 44, 139 (1976).
[13]R. W. Cahn, Contemp. Phys. 21, 43 (1980).
[14]D. J. Joyner, O. Johnson, and D. M. Hercules, J. Am. Chem. Soc. 102, 1910 (1980).
[15]O. Johnson, D. J. Joyner, and D. M. Hercules, J. Phys. Chem. 84, 542 (1980).
[16]D. J. Joyner, O. Johnson, and D. M. Hercules, J. Phys. F 10, 169 (1980).
[17]N. Lundquist, H. P. Meyers, and R. Westin, Philos. Mag. 7, 1187 (1962).
[18]R. Kuentzler, J. Phys. (Paris) 325, C1-634 (1971).
[19]R. B. Creel and R. G. Barnes, J. Chem. Phys. 56, 1549 (1972).
[20]P. J. Brown and J. L. Cox, Philos. Mag. 23, 705 (1971).
[21]R. S. Perkins and P. J. Brown, J. Phys. F 4, 906 (1974).
[22]G. V. Samsonov and B. A. Kovenskaya, in *Boron and Refractory Borides*, edited by V. I. Makovich (Springer, Berlin, 1977), pp. 5, 19.
[23]F. L. Carter, J. Less-Common Met. 47, 157 (1976).
[24]H. Taga, J. Mater. Sci. 10, 1971 (1975).
[25]G. Margaritondo, J. H. Weaver, and N. G. Stoffel, J. Phys. F 12, 662 (1979).
[26]The photoemission study of Brodén et. al. (Ref. 27) of O, C, N, and S on Fe showed peaks in the range 3.7—5.4 eV; no peaks were seen in our spectra in this region. The stability of our peaks at 6.6 and 10.5 eV eliminates CO (Refs. 28 and 29) as a possible contaminant. A wide scan synchrotron photoemission spectrum did not show the O 2*s* peak at 26.4 eV seen in B_2O_3 (Ref. 58).
[27]G. Brodén, G. Gafner, and H. P. Bonzel, Appl. Phys. 13, 333 (1977).

[28]T. Gustafsson and E. W. Plummer, in *Photoemission and the Electronic Properties of Surfaces*, edited by B. Feuerbacher, B. Fitton, and R. F. Willis (Wiley, Chichester, 1978), Chap. 12, p. 353.
[29]T. Rhodin and C. Brucker, in *Characterization of Metal and Polymer Surfaces* (Symposium), edited by L. Huang (Academic, New York, 1977), pp. 431–466.
[30]A. J. McAlister et.al. (unpublished).
[31]D. W. Bullet, J. Phys. C 11, 4501 (1978); 12, (1979); Solid State Phys. 35, 129 (1980); M. J. Kelly and D. W. Bullett, J. Phys. C 12, 2531 (1979).
[32]D. J. Joyner (unpublished).
[33]E. Antonides and G. A. Sawatzky, in *Transition Metals*, edited by M. J. G. Lee, J. M. Perz, and E. Fawcett, Inst. Phys. Conf. Ser. 39 (Institute of Physics, London, 1978), Chap. 2, p. 134.
[34]L. Yin, T. Tsang, and I. Adler, Phys. Lett. 57A (2), 193 (1976), (a) C. C. Lu, T. A. Carlson, F. B. Malik, T. C. Tucker, and C. W. Nestor, Jr., At. Data 3, 1 (1971).
[35]The peak at 16 eV in Fig. 6 for the B 2*s* density of states is due to an artifact of the Gaussian smoothing, and the B 2*s* projection should decay away smoothly without any sharp structure from 12 to 21 eV.
[36]L. Ley, O. B. Dabbousi, S. P. Kowalczyk, F. R. McFeely, and D. A. Shirley, Phys. Rev. B 16, 5372 (1977)
[37]J. Knapp, private Communication.
[38]S. T. Manson and T. W. Cooper, Phys. Rev. 165 , 126 (1968).
[39]D. J. Kennedy and S. T. Manson, Phys. Rev. A 5, 227 (1972).
[40]J. Callaway and C. S. Wang, Phys. Rev. B 16, 2095 (1977).
[41]M. Pessa, P. Heimann, and H. Neddermeyer, Phys. Rev. B 14, 3488 (1976).
[42]D. E. Eastman, F. J. Himpsel, and J. A. Knapp, Phys. Rev. Lett. 44, 95 (1980).
[43]S. T. Manson, in *Photoemission in Solids I*, edited by M. Cardona and L. Ley (Springer, Berlin, 1978).
[44]P. S. Wehner, J. Stöhr, G. Apai, F. R. McFeely, R. S. Williams, and D. A. Shirley, Phys. Rev. B 14, 2411 (1976).
[45]D. E. Eastman, in *Vacuum Ultraviolet Radiation Physics*, edited by E. E. Koch, R. Haensel, and C. Kury (Pergamon, Vieweg, 1974), p. 417.
[46]D. A. Shirley, J. Stöhr, P. S. Wehner, R. S. Williams, and G. Apai, Phys. Scr. 16, 397 (1977).
[47]P. W. Palmberg, J. Electron Spectrosc. Relat. Phenom. 5, 691 (1974).
[48]An enhancement of photoelectron intensity (cross section) has been observed for VSi_2 and $MoSi_2$ for energies above that of the np core which is considered to be a p-d resonance arising from the quantum-mechanical equivalence of several paths leading from the ground state to the final state when the photoelectron is in the continuum. These paths for the Fe $2p$-$3d$ resonance are

$$h\nu + 3p^6(4s\,3d)^n \rightarrow 3p^5(4s\,3d)^{n+1} \rightarrow 3p^6(4s\,3d)^{n-1} + \epsilon l$$

and

$$h\nu + 3p^6(4s\,3d)^n \rightarrow 3p^6(4s\,3d)^{n-1} + \epsilon l \ ,$$

where ϵl denotes the energy ϵ in the continuum. There are insufficient data points in our study to show an effect above 53.7 eV, the Fe $3p$ energy. For a discussion or resonant photoemission in transition metals, see J. H. Weaver, V. L. Moruzzi, and F. A. Schmidt, Phys. Rev. B 23, 2916 (1981); (a) L. I. Johansson, I. Lindau, M. Hecht, S. M. Goldberg, and C. S. Fadley, Phys. Rev. B 20, 4126 (1979).
[49]An alternate procedure would be to align the calculated B 2*s* and B $2p$ peaks with peaks *c* (10.5 eV) and *b* (6.6 eV), respectively. This is not a reasonable alternative since it involves a +3.2 shift for B $2p$ and a −1.9-eV shift for B 2*s*.
[50]A. Bianconi, S. B. M. Hagström, and L. Z. Bachrach, Phys. Rev. B 16, 5543 (1977).
[51]A. R. Williams and N. D. Lang, Phys. Rev. Lett. 40, 954 (1978).
[52]G. W. Rubloff, W. D. Grobman, and H. Lüth, Phys. Rev. B 14, 1450 (1976).
[53]I. Ihara, M. Hirabayashi, and M. Nakagawa, Phys. Rev. B 16, 726 (1977).
[54]M. Aono, T. Tanaka, E. Bannai, C. Oshima, and S. Kawai, Phys. Rev. B 16, 3489 (1977); M. Aono, T. C. Chang, J. A. Knapp, T. Tanaka, and D. E. Eastman, *ibid.* 21, 2661 (1980).
[55]Y. Hayasi, Sci. Rep. Tohoku Univ., Ser. 1, 51, 153 (1968).
[56]J. Cuthill, private Communication.
[57]I. I. Lyakhovskaya, T. M. Zirikina, and V. A. Fomichev, Fiz. Tverd. Tela 12, 174 (1970) [Sov. Phys. Solid State 12, 138 (1970)].
[58]D. J. Joyner and D. M. Hercules, J. Chem. Phys. 72, 1095 (1980).
[59]K. Hamrin, G. Johannson, U. Gelius, C. Nordling, and K. Siegbahn, Phys.Scr. 1, 277 (1970).
[60]A. Hasegawa and A. Yanase, J. Phys. F 7, 1245 (1977).
[61]M. Pessa, P. Heimann, and H. Neddermeyer, Phys. Rev. B 14, 3488 (1976).
[62]M. Singh, C. S. Wang, and J. Callaway, Phys. Rev. B 11, 287 (1975).
[63]E. P. Wohlfarth, Rev. Mod. Phys. 25, 211 (1953).
[64]D. G. Pettifor, Phys. Bull. 31, 202 (1980).
[65]M. B. Stearns, Phys. Rev. B 8, 4383 (1973).
[66]O. Johnson, in *Transition Metals*, Ref. 33.
[67]J. Zielinski, Phys. Status Solidi B 78, 319 (1976).
[68]O. Johnson, Phys. Status Solidi B 99, 745 (1980).
[69]A. M. Olés and K. A. Chao, Z. Phys. B35, 261 (1979); A. M. Olés, in *Transition Metals*, Conference on the Physics of Transition Metals, edited by P. Rhodes, Inst. Phys. Conf. Ser. 55 (Institute of Physics, London, 1980), p. 33.
[70]H. J. F. Jansen, D. J. Bourdreaux, and H. Snijders, Phys. Rev. B 21, 2274 (1980).
[71]P. Panissod, D. A. Guerra, A. Amamou, J. Durand, W. L. Johnson, W. L. Carter, and S. J. Poon, Phys. Rev. Lett. 44, 1465 (1980).
[72]T. Kemeny, I. Vinze, B. Fogarassy, and S. Arajs, Phys. Rev. B 20, 476 (1979).
[73]M. Matsuura, T. Nomoto, F. Itoh, and K. Suzuki, Solid State Commun. 35, 895 (1980).
[74]E. Cartier, Y. Bau, M. Liard, and H.-J. Güntherodt, J. Phys. F 10, 421 (1980).
[75]A. Amamou and G. Krill, Solid State Commun. 31, 971 (1979).
[76]D. J. Joyner and R. F. Willis, Philos. Mag. 43, 815 (1981).